Carbon Nanotube Wiring of Electrodes for High-Rate Lithium Batteries Using an Imidazolium-Based Ionic Liquid Precursor as Dispersant and Binder: A Case Study on Iron Fluoride Nanoparticles

Chilin Li,[†,*] Lin Gu,[‡,§] Jianwei Tong,[†] and Joachim Maier[†,*]

[†]Max Planck Institute for Solid State Research, Heisenbergstrasse 1, D-70569 Stuttgart, Germany, [‡]WPI Advanced Institute for Materials Research, Tohoku University, 2-1-1 Katahira, Aoba-ku, Sendai 980-8577, Japan, and [§]Institute of Physics, Chinese Academy of Sciences, Beijing 100190, People's Republic of China

ABSTRACT To meet the energy and power demands of lithium-based batteries, numerous nanostructured and -decorated material prototypes have been proposed. In particular for insulating electrodes, a decrease of grain size coupled with wiring by a conductive phase is quite effective in improving the electroactivity. In this work, we report a novel electron-wiring method using single-wall carbon nanotubes in an imidazolium-based ionic liquid precursor, which enables them to be well disentangled and dispersed, even unzipped. As a case study, *in situ* formed iron fluoride nanoparticles (~10 nm) are collected into micrometer-sized aggregates after wiring of merely 5 wt % carbon nanotubes in weight. These composite materials act as cathodes and exhibit a remarkable improvement of capacity and rate performances (e.g., 220 mAh/g at 0.1C and 80 mAh/g at 10C) due to the construction of mixed conductive networks. Therein, the ionic liquid remainder also serves as an *in situ* binder to generate a nanographene-coated fluoride, which can even run well without the addition of extra conductive carbon and binder. This nanotechnological procedure based on an ionic liquid succeeds without applying high temperature and pressure and is a significant step forward in developing high-power lithium batteries.

KEYWORDS: wiring · carbon nanotube · nanographene · ionic liquid · iron fluoride · lithium batteries

Recently, nanoengineering, especially combined with carbon decoration, has come into focus in battery research in order to facilitate simultaneous ionic and electronic transport within the electrode, to restrict grain expansion and pulverization, and hence to improve Li-storage energy and power densities, as well as long-term cycling life.[1−4] A milestone example was the commercial success of the C-$LiFePO_4$ nano structured composite cathode for lithium-ion batteries used in hybrid electric vehicles (HEVs).[5,6] It has drawn significant attention to the possibility of implementing similar other promising cathode materials, such as $LiMnPO_4$, Li_2MSiO_4 (M = Fe, Mn), or MF_3 (M = Fe, Bi), which are of low electrochemical activity in phase-pure form.[7−10] But most of the strategies focus on the coating or adsorption of conductive species on the isolated nanoparticles of active materials.[7,8,11] Electrodes made up of free-floating nanoparticles are naturally not desirable. A high proportion of extra conductive carbon and binder is typically required to reinforce intergrain contact and enhance the overall electronic conductivity. In order to address this issue, methods have been proposed to either embed active grains into the conductive matrix or directly synthesize a monolith with mesopores or macropores.[12−15] In these processes, large energy consumption, e.g., high temperature or pressure, highly erosive reagents (such as HF), or a great deal of conductive additives (up to 50 wt %) are inevitable.

In this work, we report on the preparation of an unusual single-wall carbon nanotube (SWNT) wiring using an imidazolium-based ionic liquid (IL) $BmimBF_4$ ambience. Carbon nanotubes have gained great attention in numerous fields due to excellent electrical, thermal, and mechanical properties. Nevertheless its poor dispersibility is still a difficulty, particularly in aqueous environment, leading to a limited wiring effect in lithium batteries. Recently, imidazolium-based IL was discovered to be capable of effectively disentangling SWNT clusters *via* interaction between the imidazolium cation and the π-electrons of the surface, resulting in the formation of gelatinous materials.[16,17] This physical interaction can occur without further acidic treatment, and the original

* Address correspondence to C.Li@fkf.mpg.de, S.Weiglein@fkf.mpg.de.

Received for review December 22, 2010 and accepted March 4, 2011.

Published online March 04, 2011
10.1021/nn1035608

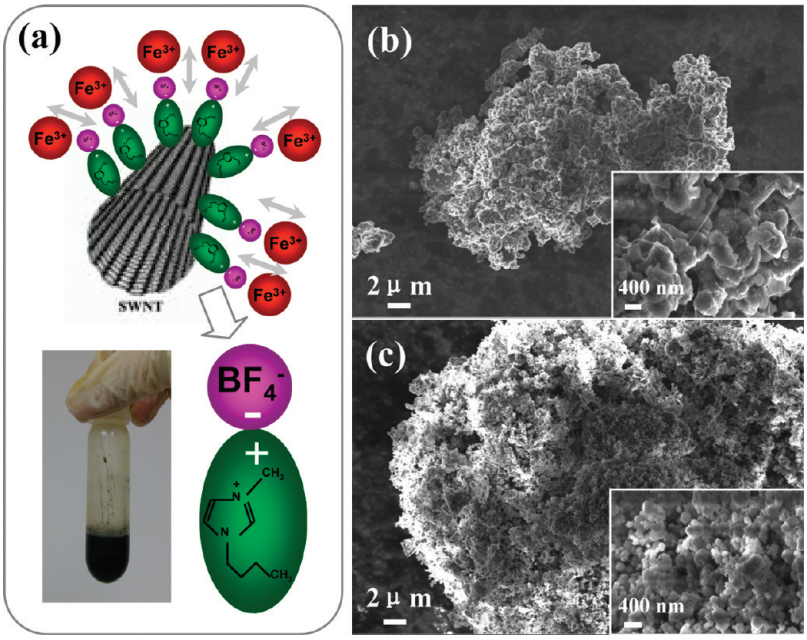

Figure 1. (a) Scheme of respective interaction of $BmimBF_4$ IL with SWNT and $Fe(NO_3)_3 \cdot 9H_2O$ precursor. Inset: Photo of SWNT-wired fluoride precipitate in IL solution. SEM images of wired (b) $FeF_{2.5} \cdot 0.5H_2O$ and (c) $FeF_3 \cdot 0.33H_2O$. Insets: Enlarged SEM images of corresponding fluoride samples.

bonding and excellent electrical properties of carbon nanotubes are not damaged or weakened. Therefore this nonaqueous wiring procedure is expected to be quite effective for battery materials, especially for those capable of chemical or physical interaction with IL.

Our previously reported iron-based fluoride cathode materials with open structure, for which the IL serves as precursor and template, are regarded as pertinent case study materials.[18,19] As most commercially available fluorides are of dense crystalline structures with marginal Li solubility, they are expected to exhibit poor rate performance even in the case of *in situ* carbon coating.[20,21] Note that ion conductivity is a prerequisite for the intercalation, multiphase transformation, and conversion reactions to occur. This shortcoming is calling for derivative fluoride cathode materials that are characterized by favorable Li-insertable channels. Though the design of expanded structures with satisfactory ion conductivity provides a new access to fluoride-based cathodes, the intrinsic electron conductivity of such open-structured fluorides is not expected to be high enough to achieve high-rate performance. Accordingly, effective wiring by highly conductive species is required to achieve a continuous electron transport network.[22,23]

For this work, the formation of conductive channels between SWNTs and fluoride nanoparticles occurs through interactions with the imidazolium ion of IL. Without the assistance of high temperature or pressure, this wiring favorable for the fabrication of micrometer-sized composite electrodes can be achieved by a very small amount of SWNT additive (5 wt %) due to its excellent dispersibility in the IL. It is believed to be especially useful for materials that are inclined to decompose or reduce under extreme synthesis conditions and the presence of carbon source. A remarkable improvement of fluoride electrochemistry is expected due to the wiring-induced construction of a mixed conductive network, which depends on the microstructure and morphology of fluorides. Moreover, the IL remainder in composite material can serve as *in situ* binder to promote the yield of nanographene-coated particles, leading to the success in the electrode free of extra conductive carbon and binder.

RESULTS AND DISCUSSION

In our route to synthesize the SWNT−fluoride composite cathodes, as shown in Figure 1a, SWNTs are uniformly decorated by $BmimBF_4$ molecules with cation orientation toward the SWNT surface. The capping function of IL significantly weakens the cross-link of SWNTs, which then are well dispersed in the IL medium. On the other hand, the outwardly stretched BF_4^- component is prone to react with the surrounding iron(III) precursor to form iron-based fluoride nanoparticles. The SWNT-wired fluoride precipitates can well suspend in IL medium (Figure 1a), in agreement with the satisfactory dispersibility of SWNT induced by IL.[16,17]

Compared with the unwired fluoride powders composed of round-shaped or sponge-type grains of hundreds of nanometers (Figure S1in the Supporting Information (SI)), the SWNT wiring greatly modifies the overall morphologies. It is expected to interfere with the intrinsic self-assembly of fluoride nanoparticles by its IL-functionalized surface adsorption ability.

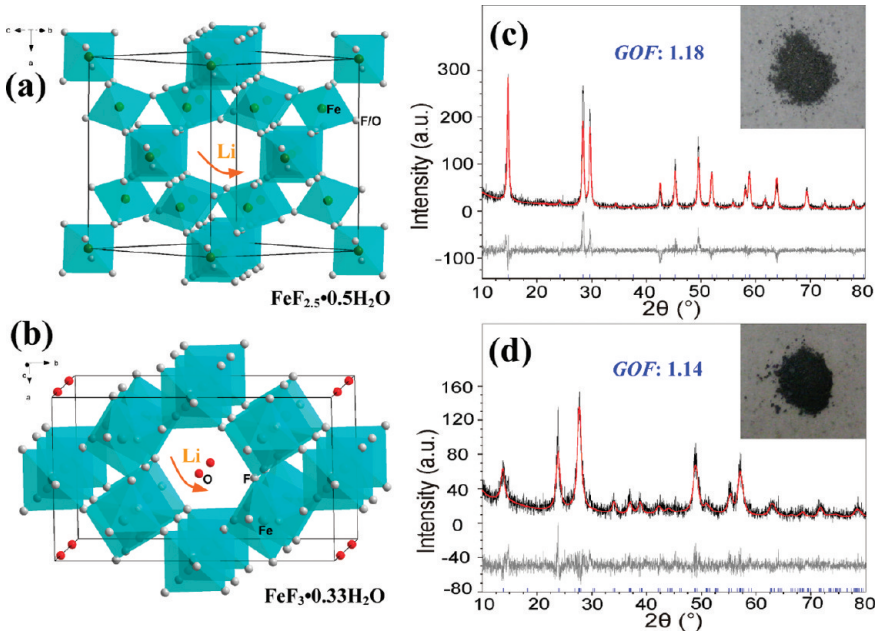

Figure 2. Structure sketches of (a) pyrochlore $FeF_{2.5}\cdot 0.5H_2O$ and (b) HTB-$FeF_3\cdot 0.33H_2O$, where one-dimensional tunnels built by hexagonal cavities are constructed to accommodate Li transport and storage. In the pyrochlore structure, FeF_6 octahedra are shown in light blue and corner-coordinated F or O atoms are shown in gray. In the HTB structure, FeF_6 octahedra are shown in light blue, corner-coordinated F atoms are shown in gray, and O atoms located in cavities are shown in red. XRD patterns and their Rietveld refinements of wired (c) pyrochlore $FeF_{2.5}\cdot 0.5H_2O$ (JCPD card no. 28-0483) and (d) HTB-$FeF_3\cdot 0.33H_2O$ (JCPD card no. 76-1262). Insets: Photos of the corresponding black powders, indicating that fine fluoride particles are uniformly embedded within SWNT-induced conductive networks.

In view of the intimate interaction between fluoride nanoparticle and SWNT *via* the bridging of IL, large composite aggregates with micrometer size are easily formed, as observed in the scanning electron microscopy (SEM) images in Figure 1b and c. They are composed of numerous grains hundreds of nanometers in size, which themselves consist of extremely small nanoparticles (~10 nm). This hierarchical structure enables the collection of free nanoparticles to enhance the volumetric energy density of lithium batteries and to avoid health hazards during practical operation. In addition, multiscale pore channels in the wiring networks are favorable for electrolyte penetration.

Generally, remarkable electron-wiring effects can be observed on materials with not exceedingly high electronic conductivities, provided that the ionic wiring is sufficient or simultaneously developed. Apart from the decrease of grain size and effective electrolyte infiltration, the intrinsic structure beneficial for Li^+ migration and storage would make an extra contribution to the electroactive enhancement. The iron-based fluorides of open structures, *viz*., pyrochlore $FeF_{2.5}\cdot 0.5H_2O$ (JCPD card no. 28-0483) and hexagonal-tungsten-bronze-type (HTB) $FeF_3\cdot 0.33H_2O$ (JCPD card no. 76-1262) (Figure 2a and b),[24,25] can be substantially improved in their performances by this strategy. From the X-ray diffraction (XRD) patterns and their Rietveld refinements (Figure 2c and d), the two fluoride phases look quite pure, with no carbon signals detected due to the small proportion of added SWNT. The detailed refinement parameters for both materials are listed in Table S1 in the SI. In both structures, six Fe octahedra are connected *via* corner-sharing to form a huge hexagonal cavity favorable for Li transport, resulting in much larger cell volumes (1123 and 710 $Å^3$ for pyrochlore and HTB structures, respectively) compared to that of the dense ReO_3-type FeF_3.[20] The main difference lies in the structural position of the hydration water molecule, which is immobilized inside the cavity for $FeF_3\cdot 0.33H_2O$ and is corner-coordinated in the $FeF_{2.5}\cdot 0.5H_2O$ by randomly substituting one-sixth of the F atoms. This substitution results in a mixed valence of the Fe ion, which was verified by electron energy-loss spectroscopy.[18] In view of the similar size of H_2O compared with F^-, the high symmetry of *Fd*3 is maintained in this ordered pyrochore structure. The different roles and degrees of freedom of hydration water in respective structures can significantly impact their conducting behavior and electrochemical activity. Herein, soft chemistry methods are thought to be exclusively useful to fabricate such fluoride phases of moderate thermostability,[18] especially in terms of our nonaqueous template synthesis for desired nanomorphologies.

The mesoscopic wiring morphology can be directly observed by high-resolution transmission electron microscopy (HRTEM) as shown in Figure 3a–d. The presence of disentangled SWNTs enables one to effectively disperse fluoride particles as small as 10 nm,

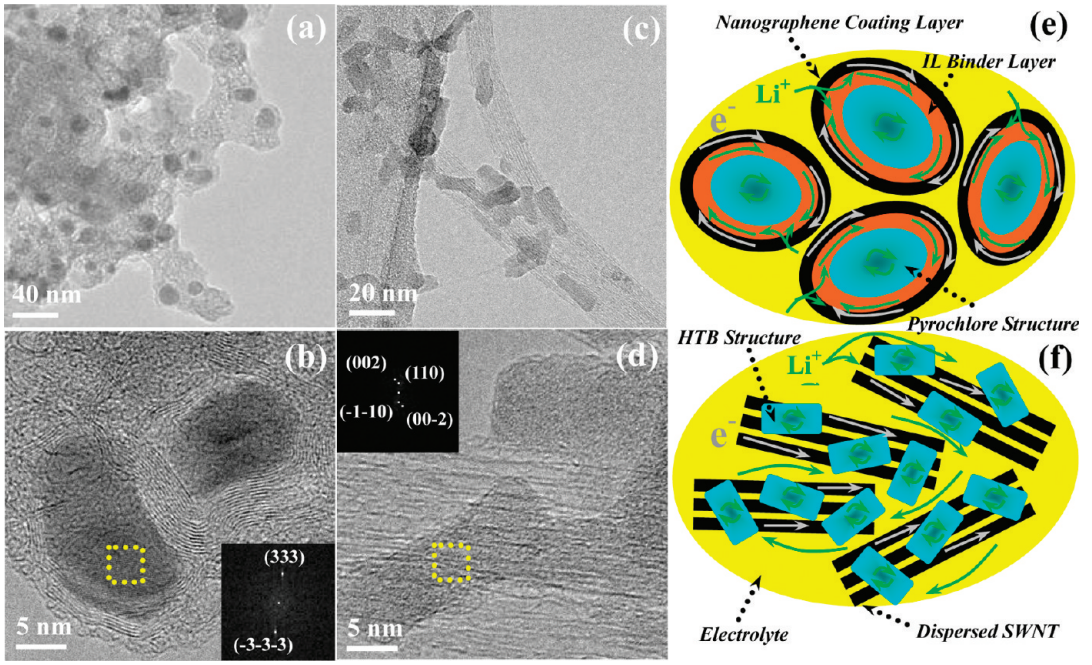

Figure 3. TEM images of (a and b) wired $FeF_{2.5}\cdot 0.5H_2O$ characterized by nanographene coating on round fluoride nanoparticles (~10 nm) and (c and d) wired $FeF_3\cdot 0.33H_2O$ characterized by loading of rectangle-shaped fluoride nanoparticles (~10 nm) on the surface of intact SWNTs at various scales. Insets of (b and d): Crystal structure diffractograms of $FeF_{2.5}\cdot 0.5H_2O$ and $FeF_3\cdot 0.33H_2O$ nanodomains, respectively. Schemes of mixed conductive networks of (e) $FeF_{2.5}\cdot 0.5H_2O$ and (f) $FeF_3\cdot 0.33H_2O$ composite electrodes.

which are otherwise prone to self-assemble into secondary particles of mesoporous structure.[18,19] Interestingly, one can observe individual round nanoparticles of $FeF_{2.5}\cdot 0.5H_2O$ uniformly embedded into the conductive medium (Figure 3a and b), wherein originally intact SWNTs are unzipped into much shorter nanoribbons (<5 nm in thickness) made up of a few graphene layers, which coat the fluoride particles. In contrast, an expected wiring behavior is observed in the SWNT-$FeF_3\cdot 0.33H_2O$ electrode (Figure 3c and d), wherein rectangular nanoparticles are distributed on the surface of perfect SWNTs. The corresponding diffractograms shown in the insets of Figure 3b and d reveal crystal symmetries that are in agreement with the XRD results.

From the Raman spectroscopy (Figure 4a), wired $FeF_3\cdot 0.33H_2O$ shows a negligible D band (~1320 cm^{-1}) compared with the G band (1500−1600 cm^{-1}), indicating good preservation of original bonding and structure of a perfect SWNT due to its nonchemical interaction with IL.[16,17] A more intensive D band can be observed in wired $FeF_{2.5}\cdot 0.5H_2O$ due to the introduction of defects during the unzipping process. But the Raman intensity ratio (~0.5) of D and G bands (I_D/I_G) is still low,[26,27] indicating high-quality graphene nanoribbons. The broadening of the 2D band (2650 cm^{-1}) further verifies the coating of multilayer graphene.

The differences of mesoscopic wiring behaviors are believed to be associated with the residual amount of IL in composite materials. From carbon−sulfur analysis, the carbon element content is ~6 and ~10 wt % in wired $FeF_3\cdot 0.33H_2O$ and $FeF_{2.5}\cdot 0.5H_2O$, respectively. Unexpectedly, the latter is almost double the designated SWNT additive amount (5%), indicating the presence of another carbon source in the IL remainder. Also, the latter exhibits much more intensive peaks in X-ray photoelectron spectroscopy (XPS) for both the N1s and B1s components (roughly 5:1 based on the

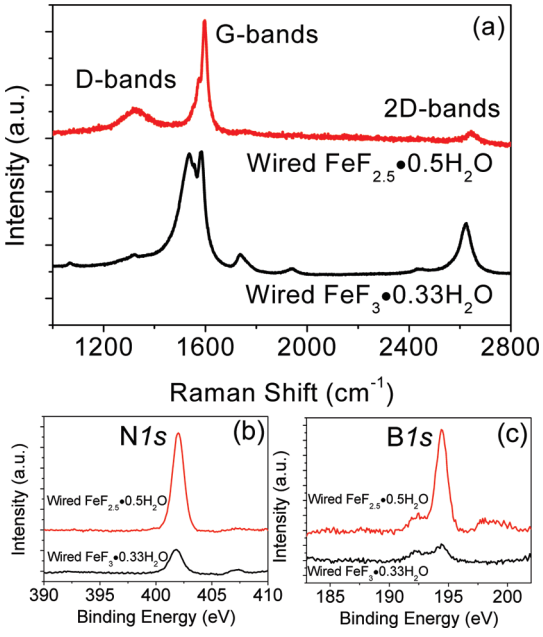

Figure 4. (a) Raman spectra of wired $FeF_{2.5}\cdot 0.5H_2O$ and $FeF_3\cdot 0.33H_2O$ samples. XPS spectra of (b) N1s and (c) B1s peaks in wired $FeF_{2.5}\cdot 0.5H_2O$ and $FeF_3\cdot 0.33H_2O$ samples.

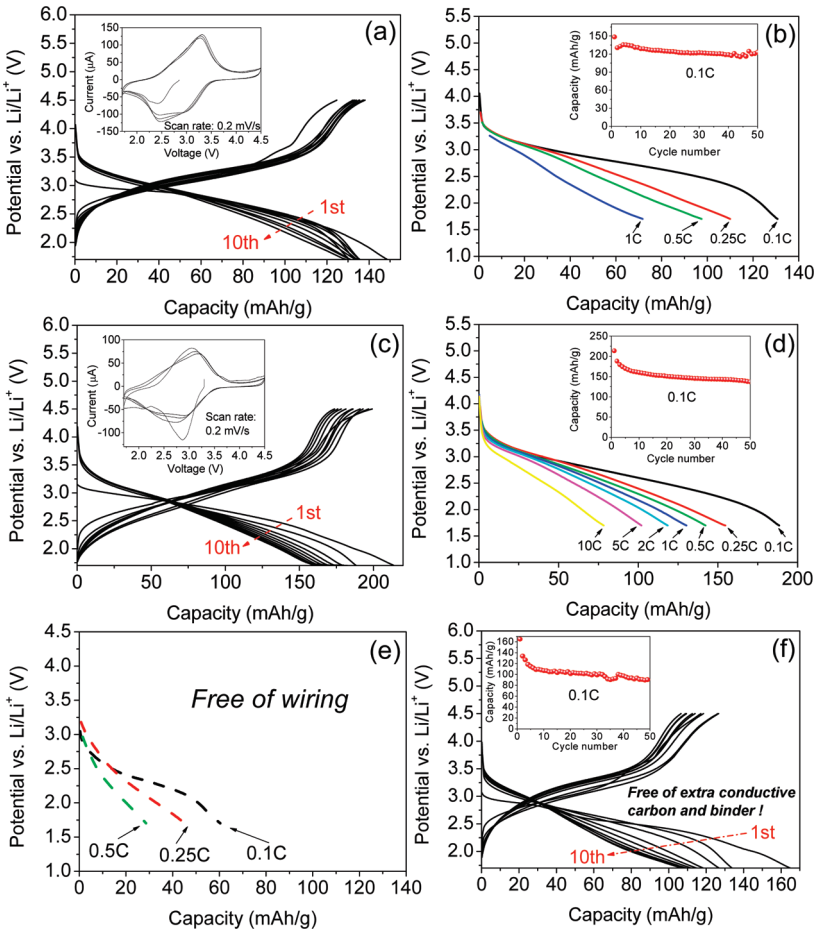

Figure 5. Voltage *vs* capacity profiles of wired (a) $FeF_{2.5}\cdot 0.5H_2O$ and (c) $FeF_3\cdot 0.33H_2O$ electrodes during the first 10 cycles with a constant rate of 0.1C. Insets: Respective cyclic voltammogram curves during the first three cycles, at a constant scanning rate of 0.2 mV/s. Voltage *vs* reversible discharge capacity profiles of (b) wired $FeF_{2.5}\cdot 0.5H_2O$, (d) wired $FeF_3\cdot 0.33H_2O$, and (e) unwired $FeF_{2.5}\cdot 0.5H_2O$ electrodes at various rates from 0.1C to 10 C. Insets of (b and d): Discharge capacity as a function of cycle number for the corresponding electrodes under the same rate of 0.1C. (f) Voltage *vs* capacity profiles of wired $FeF_{2.5}\cdot 0.5H_2O$ electrode free of extra conductive carbon and binder additives during the first 10 cycles with a constant rate of 0.1C. Inset: Discharge capacity as a function of cycle number. Voltage ranges from 1.7 to 4.5 V, and test temperature is 25 °C.

peak area for each element) of the target IL (Figure 4b and c), in good agreement with the mass ratio of non-SWNT carbon content (*viz.*, residual IL amount) in both fluorides. Additionally, a hierarchical structure can be detected in unwired $FeF_{2.5}\cdot 0.5H_2O$ (Figure S2a and S2b in SI), wherein numerous nanoparticles (~10 nm) are bound together *via* the interaction of IL remainder so as to form loose agglomerates (~300 nm) of regular round shape. Such a mesoporous morphology is also confirmed by the high Brunauer–Emmett–Teller (BET) specific surface area of 107 m^2/g (Figure S2d in the SI). After heating to 300 °C in argon, the binder component disappears, leading to free nanoparticles with similar size (Figure S2c in the SI). These results demonstrate that the intrinsic affinity of $FeF_{2.5}\cdot 0.5H_2O$ nanoparticles to IL components is likely to be much stronger. The existence of enough IL binder would promote the yield of nanographene-coated particles.

Two kinds of mixed conductive network prototypes are thus proposed (Figure 3e and f). In the $FeF_{2.5}\cdot 0.5H_2O$-wired case, both the IL binder layer and open pyrochlore structure serve as fast Li^+ migration pathways, while the highly conductive graphene coating layer provides continuous electron transport. In contrast, for the $FeF_3\cdot 0.33H_2O$-wired case, the intact SWNT plays the role of an electron artery for the surrounding-adsorbed nanoparticles, whereas the ionic path is provided by the access of the liquid electrolyte to the particles as well as by the HTB tunnel structure. In the particles themselves, the poor electronic conductivity (see below) is sufficiently high given the small particle size.

Undoubtedly, the well-defined effectively mixed conductive networks significantly improve the overall electroactivity of fluoride cathodes. The galvanostatic charge–discharge process was performed at 25 °C for both wired cathodes in a voltage range of 1.7–4.5 V as shown in Figure 5a–d. Herein, the capacity is calculated based on the composite materials. At a rate of 0.1C, initial discharge capacities of $FeF_{2.5}\cdot 0.5H_2O$ and $FeF_3\cdot 0.33H_2O$ are achieved as high as 150 and 220 mAh/g, approximately corresponding to the insertion

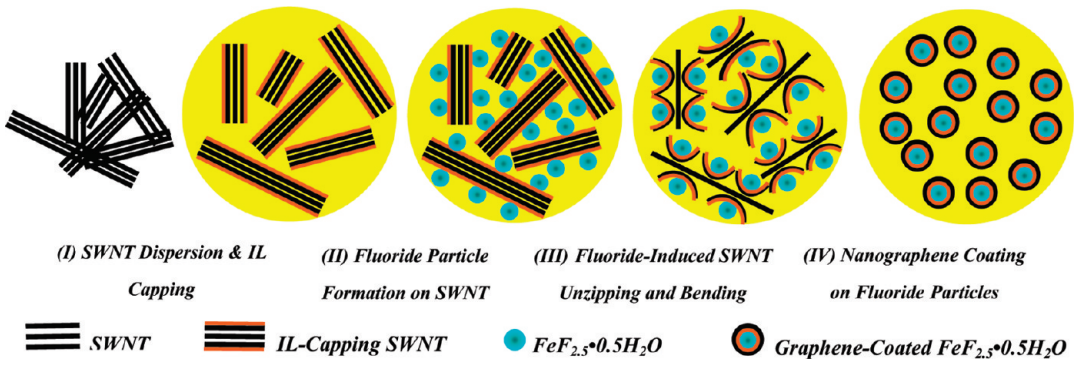

Figure 6. Route scheme of nanographene coating on $FeF_{2.5}\cdot 0.5H_2O$ nanoparticles by unzipping SWNT, utilizing imidazolium-based IL precursor as *in situ* dispersant and binder.

of 0.7 Li and 1.1 Li per formula, respectively (Figure 5a and c). In the following cycles (insets of Figure 5b and d), capacities with excellent reversibility are stabilized around 115 mAh/g (~0.5 Li) for $FeF_{2.5}\cdot 0.5H_2O$ and 143 mAh/g (~0.66 Li) for $FeF_3\cdot 0.33H_2O$, close to the respective maximum capacity in view of structural stability or mixed valence of the Fe ion.[19] As stated in our previous work on unwired $FeF_3\cdot 0.33H_2O$, 2/3 Li is likely to correspond to the capacity limit, indicating that at maximum two Li can be accommodated per one hexagonal cavity.[19] The excess capacities during the initial cycles should stem from ion adsorption or redox reaction of functional groups occurring on the surface of IL-capping SWNT.[28] Both the charge−discharge behaviors characterized by the sloped reaction plateaus around the 3 V region and low polarization reveal the solid−solution electrochemical behavior due to the facilitated Li transport within the open tunnels. These are in accordance with the cyclic voltammogram (CV) curves of both fluorides (insets of Figure 5a and c), which show similar shapes and are characterized by wide and symmetric redox peaks around the 3 V voltage region. The slightly better cycling performance for $FeF_{2.5}\cdot 0.5H_2O$ is likely to be ascribed to the more compact *in situ* nanographene coating or the less freedom of corner-coordinated hydration water molecules. Rate performance is crucial in view of the suitability of fluoride cathodes applied in high-power lithium batteries. At higher rates of 1C and 10C, $FeF_3\cdot 0.33H_2O$ exhibits reversible capacities as high as 130 and 80 mAh/g, respectively, without serious polarization degradation (Figure 5d). This is the best rate performance observed so far for fluoride-type cathode materials, to the best of our knowledge.

It is obvious that the composite materials work well in such a wide voltage range (1.7−4.5 V *vs* Li) at least at room temperature. Neither the water electrolysis plateau at 4.5 V region nor the water (or IL) reduction plateau below 2 V is observed. The long-term cycling stability also indicates sufficiently low mobility of hydrated water in the fluoride lattices and sufficiently low activity of IL remainder. In view of the reactive voltage mainly around the 3 V region, it is totally acceptable to narrow the voltage range to 2−4 V in favor of safety and compatibility with other anode materials without paying a substantial price in terms of capacity.

It should be noted that the $FeF_{2.5}\cdot 0.5H_2O$ of the pyrochlore structure is characterized by a poor electron conductivity (5.4×10^{-12} S/cm at 25 °C) with an activation energy of 0.69 eV from the electrical measurements (Figure S3 in the SI). The mismatch between electron and ion conductivities leads to unsatisfactory discharge performance for the unwired one (<60 mAh/g), along with serious polarization (Figure 5e). The poor Li-intercalation activity has also been reported for the oxide materials of the pyrochlore structure.[29] However after electron wiring, the capacity is drastically enhanced, with a remarkable decrease in polarization and increase of sustainable cycling life, and is 2 times larger than that of pure phase at the corresponding rates (Figure 5b). Similar modifications can even be observed in the wired electrode without extra carbon and binder additives (Figure 5f), indicating the good maintenance of material volume and mixed conductive network during the cycling process. Compared with traditional wiring of fluorides, where a large amount of conductive carbon additive (>15 wt %) is required to create electroactive carbon−metal−fluoride nanocomposites through high-energy ball-milling,[9,30] our wiring route is much more facile and energy-saving. Only an amount as low as 5% SWNT is required. In particular, the formation of the nanographene-coating layer further increases the efficiency of electron wires and even leads to the successful fabrication of electrodes free of additional carbon and binder.

From the discussion above, a novel nanotechnology associated with carbon coating and graphene production is generalized. As shown in Figure 6, at the initial stages, fluoride nanoparticles are enabled to be nucleated and adhered at the IL-capping layers of individual SWNT surfaces spontaneously, rather than

gathering up each other. Interestingly, the affinity of the fluoride particle surface to IL layers gradually promotes the unzipping of loaded SWNTs into graphene nanoribbons, which further bend and encircle the fluoride nanoparticles. Obviously unzipping of SWNTs followed by formation of a core−shell structure is intimately associated with the strong affinities of the IL with the fluoride and the SWNT, respectively. The extremely small size of the fluoride nanoparticles may also be one of the key factors to promote the SWNT unzipping into such small graphene fragments. Further questions concerning the catalytic role of the fluoride nanoparticles or the initial steps of the unzipping mechanism are currently under investigation.

In contrast to traditional carbon-coating methods,[11,31,32] such as pyrolysis of carbonaceous precursors, the whole process is carried out under very mild conditions free of high temperature, high pressure, or use of extra catalyst. This strategy of a highly graphitized thin carbon (nanographene) coating is highly desired for high-performance electrode materials,[33,34] but has been rarely reported compared with disordered or amorphous carbon coating.[11] This method is extendable to other electrode materials provided that their surfaces are radical-functionalized to create enough attraction force to target ILs. In addition, graphene nanoribbons themselves are attracting attention recently due to their unique electron properties, but their fabrication is still a challenge. Compared with some recent works on unzipping carbon nanotubes into narrow graphene nanoribbons,[26,27,35] our facile route does not require additional oxidation/reduction or etching steps, desirably leading to high-quality products (see Raman spectra in Figure 4a). Once the nanotemplates (such as fluoride particles here) can be removed, pure graphene-based substances would be obtained.

CONCLUSIONS

In summary, a carbon nanotube wiring technique, characterized by the decoration of imidazolium-based IL as *in situ* dispersant and binder, is successfully designed to develop high-performance and high-tap-density composite electrodes of lithium batteries. Nanostructured metal fluorides where the F source is provided by the same IL are shown to be good wiring prototypes, in view of their intrinsically low electronic conductivity, multilevel interaction with SWNT (*e.g.*, charge transfer, morphology match), and significant potential as cathode materials. This wiring is expected to be extended to a wide range of functional materials, with the prerequisite of introducing physical or chemical interactions of them with target ILs.

EXPERIMENTAL SECTION

Nanowired iron-based fluorides with various amounts of hydration water were synthesized by ionic liquid 1-butyl-3-methylimidazolium tetrafluoroborate ($BmimBF_4$) (Aldrich, >98%) and iron(III) nitrate nonahydrate ($Fe(NO_3)_3\cdot 9H_2O$) precursor powder (Aldrich, 99.99%) under the participation of well-dispersed single-wall carbon nanotubes grown by laser ablation (Sineurope Nanotech). The nonaqueous precipitation method for pure fluoride phases and its synthesis mechanism have been described elsewhere.[18] At first, a certain amount of SWNT cluster (5% in composition electrode weight) was added into 10 mL of $BmimBF_4$, which then was agitated at 50 °C for 1 h, to form a uniform black solvent. Therein, well-dispersed SWNTs were decorated by the imidazolium ion of IL on the surface. Then, 1 g of $Fe(NO_3)_3\cdot 9H_2O$, which provides iron and hydration water for $BmimBF_4$ hydrolysis, was gradually added to the SWNT-suspended IL solvent in an agitation state. For the preparation of wired $FeF_{2.5}\cdot 0.5H_2O$, the solution was continuously agitated at 50 °C for 12 h, until composite precipitates were completely formed. Apart from a prior vacuum treatment for 2 h to remove a certain extent of hydration water, the synthesis of wired $FeF_3\cdot 0.33H_2O$ was carried out under similar conditions. These products were washed with acetone and centrifuged at 6000 rpm five times to remove residual ionic liquid and other organic impurities, followed by subsequent drying under vacuum at 80 °C for 20 h. The exact carbon content in wired materials was detected by a Carbon Sulfur Determinator (Eltra, CS800).

Structure and crystallinity of wired iron-based fluoride powders were checked by X-ray diffraction using a Philips PW3710 (40 kV/30 mA) diffractometer with Cu Kα radiation. The peak profile and precise lattice parameters of the electrode patterns were determined by Rietveld refinement using the TOPAS program. The electrode morphologies were investigated by a JEOL 6300F field-emission scanning electron microscope (JEOL, Tokyo, Japan) operated at 15 keV. High-resolution transmission electron microscopy and selected-area electron diffraction measurements were carried out using a JEOL 4000EX transmission electron microscope operated at 400 keV (JEOL, Tokyo, Japan). Raman spectra were recorded on a Jobin Yvon LabRam spectrometer (excitation wavelength: 632.8 nm) to detect the graphitization degree of carbon allotropes. X-ray photoelectron spectroscopy (XPS) with an Axis Ultra instrument (Kratos Analytical Ltd., UK) was performed to estimate the residual IL content in electrode materials. The Brunauer−Emmett−Teller method was used to calculate the specific surface area and pore diameter distribution. The nitrogen sorption isotherms were obtained with an Autosorb-1 system (Quanta Chrome).

Two-electrode Swagelok-type cells were assembled with wired (or unwired) iron-based fluorides as working electrode and high-purity lithium foil (Aldrich) as counter electrode. The working electrodes were prepared by mixing iron-based fluorides, carbon black, and poly(vinyl difluoride) with a weight ratio of 80:10:10, which were then pasted on pure titanium foil (99.6%, Goodfellow) followed by drying under vacuum at 80 °C for 20 h. Some electrodes were also prepared without the extra conductive carbon and binder additives. Glass fiber (GF/D) from Whatman was employed as the separator. The electrolyte involves 1 M $LiPF_6$ in a nonaqueous mixture of ethylene carbonate and dimethyl carbonate with a volume ratio of 1:1 (Ube Industries Ltd.). The cells were assembled in an Ar-filled glovebox. Charge−discharge measurements of iron-based fluoride cathodes *vs* Li/Li^+ were performed at room temperature under different rates (0.1C−10C) in a voltage range of 1.7−4.5 V on an Arbin MSTAT battery test system. Cyclic voltammogram measurements were carried out at a constant scanning rate of 0.2 mV/s in the same voltage range of 1.7−4.5 V on a Solartron SI 1287 electrochemical interface. For the investigation of electrical conductivity, the as-synthesized powder samples were pelletized by isostatical pressing at 800 kN. A

typical pellet had a diameter of about 5.5 mm and a thickness of about 0.9 mm. Platinum thin films were then sputtered on both sides of the pellet to serve as electronic electrodes. Alternating current impedance measurements were carried out by a high-resolution dielectric analyzer (Novocontrol) in a frequency range from 2×10^6 to 1 Hz, from room temperature to 150 °C in air. Direct current polarization measurement was performed at a current of 0.00001 μA under galvanostatic conditions.

Acknowledgment. The authors thank V. Duppel, G. Götz, B. Fenk, A. Fuchs, A. Schulz, and M. Konuma for their technical help in TEM, XRD, SEM, BET, Raman, and XPS measurements.

Supporting Information Available: SEM of unwired fluorides, Rietveld refinement parameters for wired fluorides, TEM and BET of unwired $FeF_{2.5} \cdot 0.5H_2O$ with different heating treatment, and ac impedance, dc polarization, and Arrhenius plots of pure $FeF_{2.5} \cdot 0.5H_2O$ pellets. This material is available free of charge *via* the Internet at http://pubs.acs.org.

REFERENCES AND NOTES

1. Maier, J. Nanoionics: Ion Transport and Electrochemical Storage in Confined Systems. *Nat. Mater.* **2005,** *4*, 805–815.
2. Bruce, P. G.; Scrosati, B.; Tarascon, J. M. Nanomaterials for Rechargeable Lithium Batteries. *Angew. Chem., Int. Ed.* **2008,** *47*, 2930–2946.
3. Guo, Y. G.; Hu, J. S.; Wan, L. J. Nanostructured Materials for Electrochemical Energy Conversion and Storage Devices. *Adv. Mater.* **2008,** *20*, 2878–2887.
4. Li, H.; Wang, Z. X.; Chen, L. Q.; Huang, X. J. Research on Advanced Materials for Li-Ion Batteries. *Adv. Mater.* **2009,** *21*, 4593–4607.
5. Padhi, A. K.; Nanjundaswamy, K. S.; Goodenough, J. B. Phospho-Olivines as Positive-Electrode Materials for Rechargeable Lithium Batteries. *J. Electrochem. Soc.* **2003,** *150*, 1188–1194.
6. Huang, H.; Yin, S. C.; Nazar, L. F. Approaching Theoretical Capacity of $LiFePO_4$ at Room Temperature at High Rates. *Electrochem. Solid-State Lett.* **2001,** *4*, A170–A172.
7. Martha, S. K.; Markovsky, B.; Grinblat, J.; Gofer, Y.; Haik, O.; Zinigrad, E.; Aurbach, D.; Drezen, T.; Wang, D.; Deghenghi, G.; *et al*. $LiMnPO_4$ as an Advanced Cathode Material for Rechargeable Lithium Batteries. *J. Electrochem. Soc.* **2009,** *156*, A541–A552.
8. Muraliganth, T.; Stroukoff, K. R.; Manthiram, A. Microwave-Solvothermal Synthesis of Nanostructured Li_2MSiO_4/C (M = Mn and Fe) Cathodes for Lithium-Ion Batteries. *Chem. Mater.* **2010,** *22*, 5754–5761.
9. Badway, F.; Pereira, N.; Cosandey, F.; Amatucci, G. G. Carbon-Metal Fluoride Nanocomposites - Structure and Electrochemistry of FeF_3:C. *J. Electrochem. Soc.* **2003,** *150*, A1209–A1218.
10. Bervas, M.; Badway, F.; Klein, L. C.; Amatucci, G. G. Bismuth Fluoride Nanocomposite as a Positive Electrode Material for Rechargeable Lithium Batteries. *Electrochem. Solid-State Lett.* **2005,** *8*, A179–A183.
11. Hu, Y. S.; Demir-Cakan, R.; Titirici, M. M.; Muller, J. O.; Schlogl, R.; Antonietti, M.; Maier, J. Superior Storage Performance of a Si@SiO_x/C Nanocomposite as Anode Material for Lithium-Ion Batteries. *Angew. Chem., Int. Ed.* **2008,** *47*, 1645–1649.
12. Hassoun, J.; Derrien, G.; Panero, S.; Scrosati, B. A Nanostructured Sn-C Composite Lithium Battery Electrode with Unique Stability and High Electrochemical Performance. *Adv. Mater.* **2008,** *20*, 3169–3175.
13. Yu, Y.; Gu, L.; Zhu, C. B.; Tsukimoto, S.; van Aken, P. A.; Maier, J. Reversible Storage of Lithium in Silver-Coated Three-Dimensional Macroporous Silicon. *Adv. Mater.* **2010,** *22*, 2247–2250.
14. Dominko, R.; Bele, M.; Gaberscek, M.; Remskar, M.; Hanzel, D.; Goupil, J. M.; Pejovnik, S.; Jamnik, J. Porous Olivine Composites Synthesized by Sol-Gel Technique. *J. Power Sources* **2006,** *153*, 274–280.
15. Doherty, C. M.; Caruso, R. A.; Smarsly, B. M.; Adelhelm, P.; Drummond, C. J. Hierarchically Porous Monolithic $LiFePO_4$/Carbon Composite Electrode Materials for High Power Lithium Ion Batteries. *Chem. Mater.* **2009,** *21*, 5300–5306.
16. Fukushima, T.; Kosaka, A.; Ishimura, Y.; Yamamoto, T.; Takigawa, T.; Ishii, N.; Aida, T. Molecular Ordering of Organic Molten Salts Triggered by Single-Walled Carbon Nanotubes. *Science* **2003,** *300*, 2072–2074.
17. Fukushima, T.; Aida, T. Ionic Liquids for Soft Functional Materials with Carbon Nanotubes. *Chem.—Eur. J.* **2007,** *13*, 5048–5058.
18. Li, C. L.; Gu, L.; Tsukimoto, S.; van Aken, P. A.; Maier, J. Low Temperature Ionic-Liquid-Based Synthesis of Nanostructured Iron-Based Fluoride Cathodes for Lithium Batteries. *Adv. Mater.* **2010,** *22*, 3650–3654.
19. Li, C. L.; Gu, L.; Tong, J. W.; Tsukimoto, S.; Maier, J. A Mesoporous Iron-Based Fluoride Cathode of Tunnel Structure for Rechargeable Lithium Batteries. *Adv. Funct. Mater.* 10.1002/adfm.201002213.
20. Yamakawa, N.; Jiang, M.; Key, B.; Grey, C. P. Identifying the Local Structures Formed during Lithiation of the Conversion Material, Iron Fluoride, in a Li Ion Battery: A Solid-State NMR, X-Ray Diffraction, and Pair Distribution Function Analysis Study. *J. Am. Chem. Soc.* **2009,** *131*, 10525–10536.
21. Doe, R. E.; Persson, K. A.; Meng, Y. S.; Ceder, G. First-Principles Investigation of the Li-Fe-F Phase Diagram and Equilibrium and Nonequilibrium Conversion Reactions of Iron Fluorides with Lithium. *Chem. Mater.* **2008,** *20*, 5274–5283.
22. Hu, Y. S.; Guo, Y. G.; Dominko, R.; Gaberscek, M.; Jamnik, J.; Maier, J. Improved Electrode Performance of Porous $LiFePO_4$ Using RuO_2 as an Oxidic Nanoscale Interconnect. *Adv. Mater.* **2007,** *19*, 1963–1966.
23. Guo, Y. G.; Hu, Y. S.; Sigle, W.; Maier, J. Superior Electrode Performance of Nanostructured Mesoporous TiO_2 (Anatase) through Efficient Hierarchical Mixed Conducting Networks. *Adv. Mater.* **2007,** *19*, 2087–2091.
24. De Pape, R.; Ferey, G. A New Form of FeF_3 with the Pyrochlore Structure: Soft Chemistry Synthesis, Crystal Structure, Thermal Transitions and Structural Correlations with the Other Forms of FeF_3. *Mater. Res. Bull.* **1986,** *21*, 971–978.
25. Le Blanc, M.; Ferey, G.; Chevallier, P.; Calage, Y.; De Pape, R. Hexagonal Tungsten Bronze-Type FeIII Fluoride: $(H_2O)_{0.33}FeF_3$; Crystal Structure, Magnetic Properties, Dehydration to a New Form of Iron Trifluoride. *J. Solid State Chem.* **1983,** *47*, 53–58.
26. Jiao, L. Y.; Zhang, L.; Wang, X. R.; Diankov, G.; Dai, H. J. Narrow Graphene Nanoribbons from Carbon Nanotubes. *Nature* **2009,** *458*, 877–880.
27. Jiao, L. Y.; Wang, X. R.; Diankov, G.; Wang, H. L.; Dai, H. J. Facile Synthesis of High-Quality Graphene Nanoribbons. *Nat. Nanotechnol.* **2010,** *5*, 321–325.
28. Lee, S.-W.; Yabuuchi, N.; Gallant, B. M.; Chen, S.; Kim, B. S.; Hammond, P. T.; Shao-Horn, Y. High-Power Lithium Batteries from Functionalized Carbon-Nanotube Electrodes. *Nat. Nanotechnol.* **2010,** *5*, 531–537.
29. Rabanal, M. E.; Varez, A.; Amador, U.; Dompablo, E. A.; Garcia-Alvarado, F. Structure and Reaction with Lithium of Tetragonal Pyrochlore-Like Compound $Sm_2Ti_2O_7$. *J. Mater. Proc. Tech.* **1999,** *93*, 529–533.
30. Nishijima, M.; Gocheva, I. D.; Okada, S.; Doi, T.; Yamaki, J.; Nishida, T. Cathode Properties of Metal Trifluorides in Li and Na Secondary Batteries. *J. Power Sources* **2009,** *190*, 558–562.
31. Gao, P. F.; Fu, J. W.; Yang, J.; Lv, R. G.; Wang, J. L.; Nuli, Y. N.; Tang, X. Z. Microporous Carbon Coated Silicon Core/Shell Nanocomposite *via in situ* Polymerization for Advanced Li-Ion Battery Anode Material. *Phys. Chem. Chem. Phys.* **2009,** *11*, 11101–11105.
32. Adelhelm, P.; Hu, Y. S.; Antonietti, M.; Maier, J.; Smarsly, B. M. Hollow Fe-Containing Carbon Fibers with Tubular Tertiary Structure: Preparation and Li-Storage Properties. *J. Mater. Chem.* **2009,** *19*, 1616–1620.

33. Wang, K. X.; Li, Z. L.; Wang, Y. G.; Liu, H. M.; Chen, J. S.; Holmes, J.; Zhou, H. S. Carbon Nanocages with Nanographene Shell for High-Rate Lithium Ion Batteries. *J. Mater. Chem.* **2010,** *20*, 9748–9753.
34. Yang, S. B.; Feng, X. L.; Zhi, L. J.; Cao, Q.; Maier, J.; Mullen, K. Nanographene-Constructed Hollow Carbon Spheres and Their Favorable Electroactivity with Respect to Lithium Storage. *Adv. Mater.* **2010,** *22*, 838–842.
35. Kosynkin, D. V.; Higginbotham, A. L.; Sinitskii, A.; Lomeda, J. R.; Dimiev, A.; Price, B. K.; Tour, J. M. Longitudinal Unzipping of Carbon Nanotubes to Form Graphene Nanoribbons. *Nature* **2009,** *458*, 872–876.